

Supporting Information

Hierarchical Cu(OH)₂@Ni₂(OH)₂CO₃ Core/shell Nanowire Arrays *in situ* Growth on Three-dimensional Copper Foam for High- 5 performance Solid-state Supercapacitors

Sheng Zhu, Zidan Wang, Fangzhi Huang, Hui Zhang, Shikuo Li*

Lab of Clean Energy & Environmental Catalysis, School of Chemistry and Chemical Engineering, Anhui University, Hefei 230601, China

Received (in XXX, XXX) Xth XXXXXXXXX 20XX, Accepted Xth XXXXXXXXX 20XX

10 DOI: 10.1039/b000000x

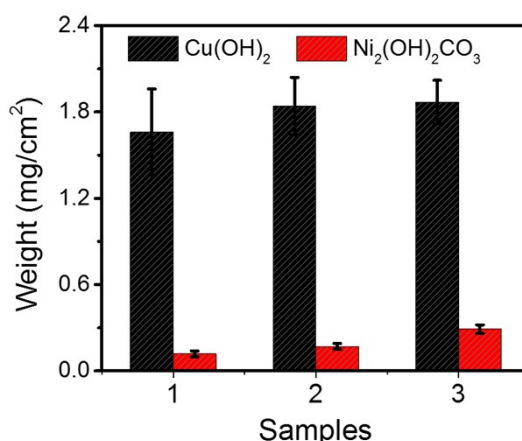


Figure S1. Different mass contents of Cu(OH)₂ and Ni₂(OH)₂CO₃ from different Cu(OH)₂@Ni₂(OH)₂CO₃ samples measured by atomic absorption.

A piece of 1×1×0.12 cm³ 3D copper foam with hierarchical Cu(OH)₂@Ni₂(OH)₂CO₃ core/shell nanowire arrays was first soaked in 100 ml concentrated HCl solution under ultrasonic condition to thoroughly dissolve the surfaced active materials, which was then diluted into 15 1L solution for atomic absorption measurements. The measured values for Cu and Ni elements were 0.0633, 0.0025 mg L⁻¹, respectively. The real volume of the 1×1×0.12 cm³ 3D copper foam was about 0.054 cm³ by dipping method. The mass contents of Cu(OH)₂ and Ni₂(OH)₂CO₃ on the substrates were calculated by the following formula:

$$w = \frac{\frac{A \times V}{M_m} \times M_{mx}}{V'} = \frac{A \times V}{M_m} \times M_{mx} \times \frac{d}{V'}$$

where A represents the value by atomic absorption measurement, V is volume of the solution (1 L), M_m represents the molar mass of Cu 20 or Ni elements, M_{mx} is molar mass of Cu(OH)₂ and Ni₂(OH)₂CO₃, V' is the real volume and d is the thickness of the copper foam. Thus, the total mass contents of Cu(OH)₂ and Ni₂(OH)₂CO₃ on the copper foams were calculated as 1.8 and 0.3 mg cm⁻².

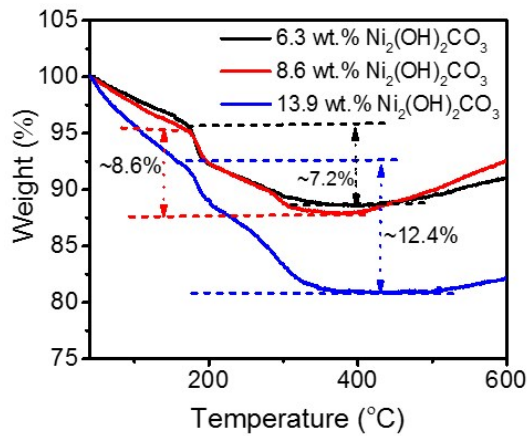
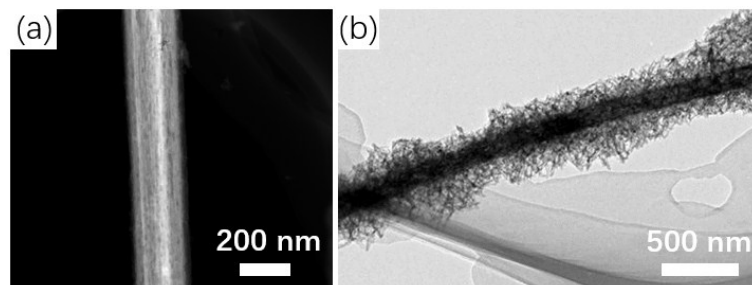


Figure S2. (a) TG curves of $\text{Cu}(\text{OH})_2$, $\text{Ni}_2(\text{OH})_2\text{CO}_3$ and $\text{Cu}(\text{OH})_2@\text{Ni}_2(\text{OH})_2\text{CO}_3$ samples, (b) TG curves of the hierarchical samples with different $\text{Ni}_2(\text{OH})_2\text{CO}_3$ mass contents.



5

Figure S3. TEM images of (a) the pristine $\text{Cu}(\text{OH})_2$, (b) typical $\text{Cu}(\text{OH})_2@\text{Ni}_2(\text{OH})_2\text{CO}_3$ hierarchical nanowires.

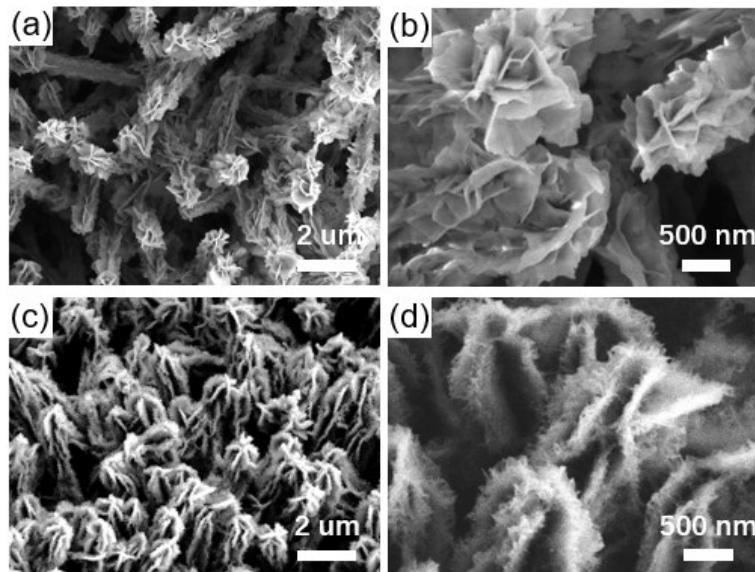


Figure S4. SEM images (a, b) of the as-obtained hierarchical samples with 6.3 wt.% $\text{Ni}_2(\text{OH})_2\text{CO}_3$ content, and (c, d) 8.6 wt.% $\text{Ni}_2(\text{OH})_2\text{CO}_3$ content.

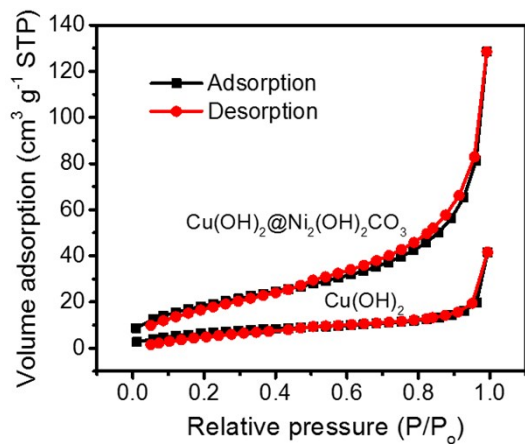
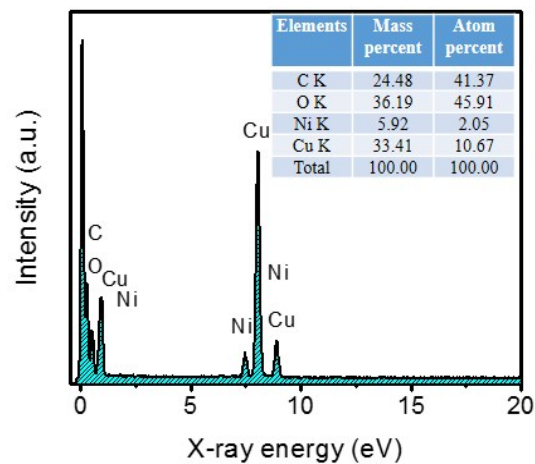


Figure S5. Nitrogen adsorption–desorption isotherms of the pristine $\text{Cu}(\text{OH})_2$ and typical $\text{Cu}(\text{OH})_2@\text{Ni}_2(\text{OH})_2\text{CO}_3$ samples.



5

Figure S6. EDX spectra of the typical $\text{Cu}(\text{OH})_2@\text{Ni}_2(\text{OH})_2\text{CO}_3$ hierarchical sample.

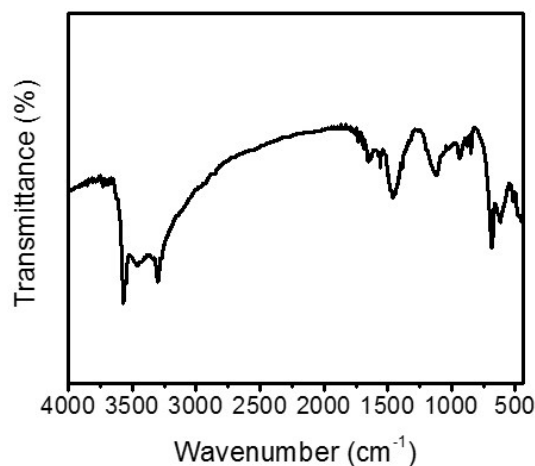


Figure S7. FT-IR spectrum of the typical $\text{Cu}(\text{OH})_2@\text{Ni}_2(\text{OH})_2\text{CO}_3$ hierarchical sample.

10

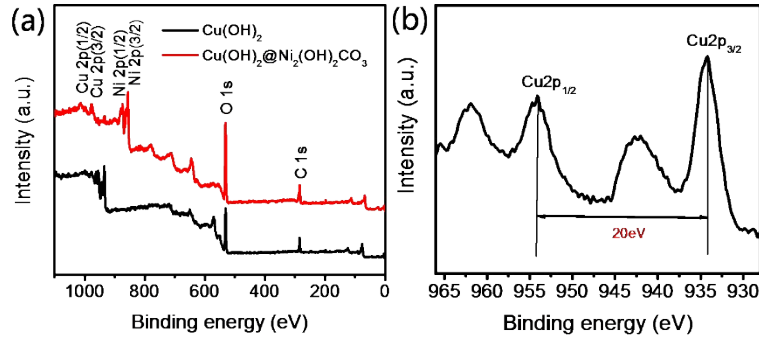
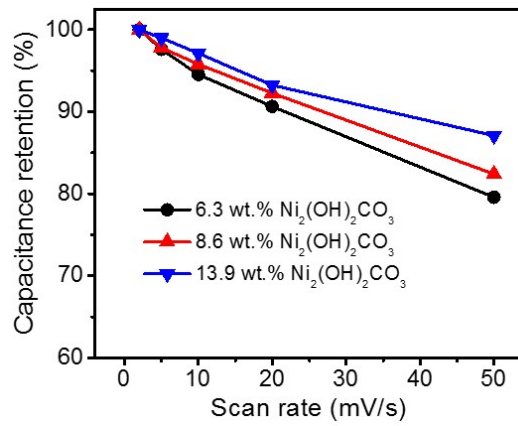


Figure S8. (a) XPS survey spectra of the pristine $\text{Cu}(\text{OH})_2$ and the hierarchical $\text{Cu}(\text{OH})_2@\text{Ni}_2(\text{OH})_2\text{CO}_3$ core/shell samples, (b) XPS spectra of Cu 2p from the pristine $\text{Cu}(\text{OH})_2$ sample.



5

Figure S9. (a) GCD curves of the hierarchical samples with different $\text{Ni}_2(\text{OH})_2\text{CO}_3$ mass contents under current density of 1.0 mA cm^{-2} .

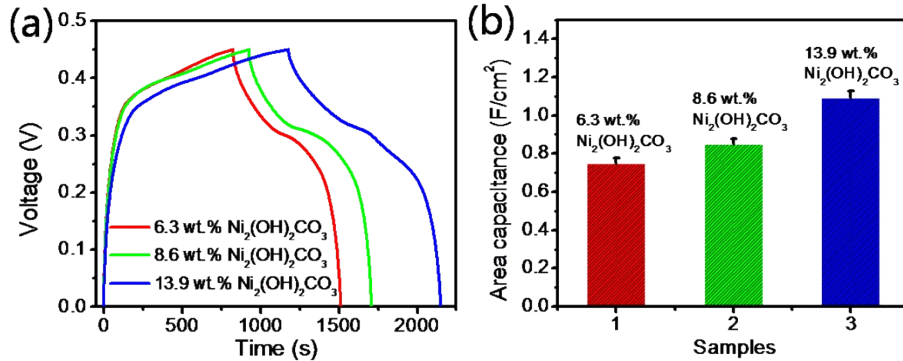


Figure S10. Capacitance retention of the hierarchical samples with different $\text{Ni}_2(\text{OH})_2\text{CO}_3$ mass contents at various scan rates.

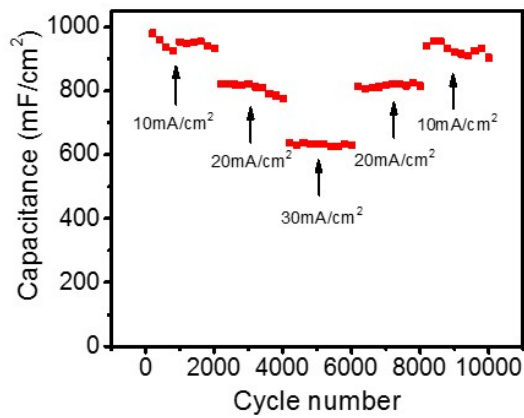
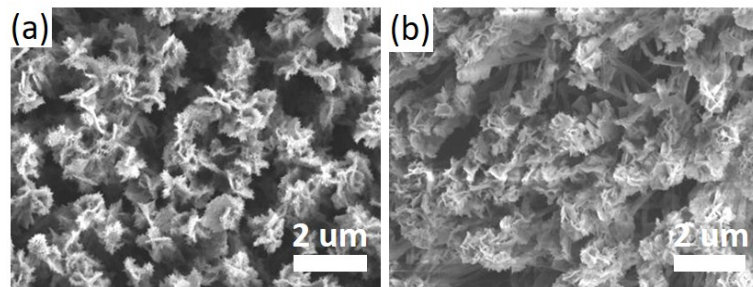


Figure S11. Cycling performance of the typical $\text{Cu}(\text{OH})_2@\text{Ni}_2(\text{OH})_2\text{CO}_3$ hierarchical sample under various current densities.



5

Figure S12. SEM images of the typical $\text{Cu}(\text{OH})_2@\text{Ni}_2(\text{OH})_2\text{CO}_3$ sample (a) before and (b) after cycling for 10000 cycles.

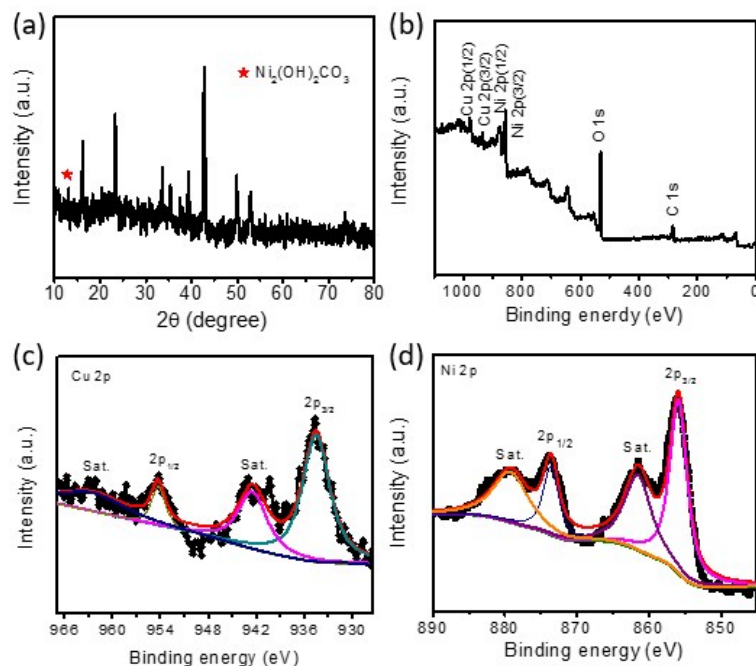


Figure S13. (a) XRD patterns of the typical $\text{Cu}(\text{OH})_2@\text{Ni}_2(\text{OH})_2\text{CO}_3$ hierarchical sample after 10000 cycles. XPS survey spectra of $\text{Cu}(\text{OH})_2@\text{Ni}_2(\text{OH})_2\text{CO}_3$ hierarchical sample after 10000 cycles (b), (c) $\text{Cu} 2\text{p}$, and (d) $\text{Ni} 2\text{p}$.

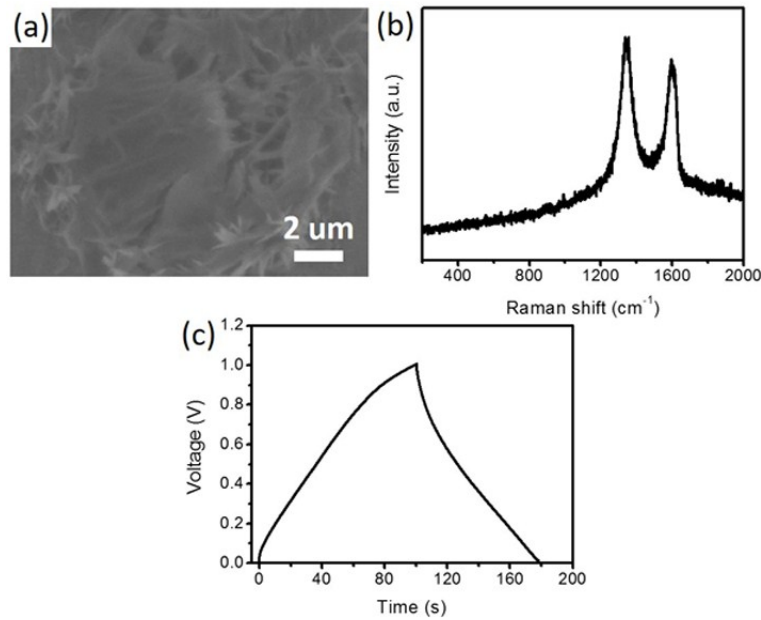


Figure S14. (a) SEM image of rGO on copper foam, (b) Raman pattern of rGO, (c) GCD curve of rGO on copper foam electrode at a current density of 1 mA cm^{-2} .

5

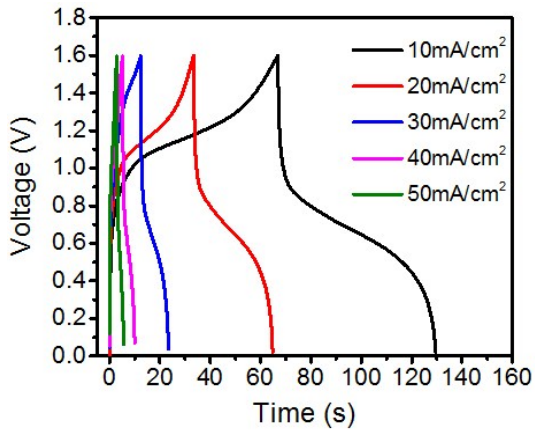


Figure S15. GCD curves of the $\text{Cu(OH)}_2 @ \text{Ni}_2(\text{OH})_2\text{CO}_3 / \text{rGO}$ asymmetric supercapacitor under different current densities at the potential range from 0 to 1.6 V.

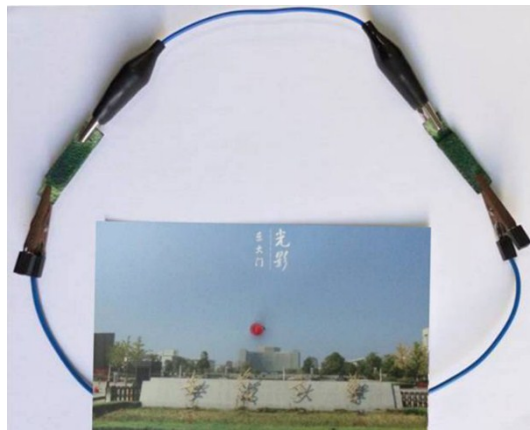


Figure S16. A device consisted by a red LED indicator and two Cu(OH)₂@Ni₂(OH)₂CO₃/rGO asymmetric devices in series.

Table S1. The detailed ESR values of different electrodes.

Sample	Cu(OH) ₂	Ni ₂ (OH) ₂ CO ₃	Cu(OH) ₂ @Ni ₂ (OH) ₂ CO ₃
Rct [ohm]	4.9	5.6	2.5
Normalized data	0.8	1.0	0

5

10

15

20

Table S2. Comparison of the properties for as-prepared Cu(OH)₂@Ni₂(OH)₂CO₃/rGO asymmetric supercapacitor with these nickel based asymmetric SCs in published papers.

Asymmetric SCs	PENS ^{a)}	C _s	Scan rate	E _{max}	P _{max}	Ref.
NiMoO ₄ //AC ^{b)}	NSs	151.7 F g ⁻¹	1 A g ⁻¹	60.9 Wh kg ⁻¹	850 W kg ⁻¹	[1]
MnO ₂ /NiO//rGO	HNWAs ^{c)}	218 F g ⁻¹	3 A g ⁻¹	59.5 Wh kg ⁻¹	2.1 kW kg ⁻¹	[2]
H-TiO ₂ @Ni(OH) ₂ //N-C ^{d)}	HNWAs	150.6 F g ⁻¹	1 A g ⁻¹	70.9 Wh kg ⁻¹	102.9 W kg ⁻¹	[3]
NiCo ₂ S ₄ @Ni(OH) ₂ //AC	HNSAs ^{e)}	132.7 F g ⁻¹	5 mA cm ⁻²	52.3 Wh kg ⁻¹	290.0 W kg ⁻¹	[4]
Co ₃ O ₄ @Ni(OH) ₂ //rGO	HNWAs	110.8 F g ⁻¹	2.5 mA cm ⁻²	41.8 Wh kg ⁻¹	33.5 W kg ⁻¹	[5]
Ni-Co _{1.5} -O//RGO@Fe ₃ O ₄	HMSs ^{f)}	132.6 F g ⁻¹	1 A g ⁻¹	41.5 Wh kg ⁻¹	505 W kg ⁻¹	[6]
NiCo ₂ O ₄ @Co _{0.33} Ni _{0.67} (OH) ₂ //CMK ^{g)} -3	HNSAs	87.9 F g ⁻¹	5 mA cm ⁻²	31.2 Wh kg ⁻¹	396 W kg ⁻¹	[7]
CoNi ₃ O ₄ /C//AC	HNWAs	64.7 F g ⁻¹	1.0 mA cm ⁻²	20.1 Wh kg ⁻¹	130.4 W kg ⁻¹	[8]
NiCo ₂ O ₄ @MnO ₂ //AC	HNWAs	112.0 F g ⁻¹	1.0 mA cm ⁻²	35.0 Wh kg ⁻¹	163 W kg ⁻¹	[9]
NiCo ₂ S ₄ @Ni ₃ V ₂ O ₈ //AC	HNWAs	93.8 F g ⁻¹	1 A g ⁻¹	42.7 Wh kg ⁻¹	200.0 W kg ⁻¹	[10]
Cu(OH) ₂ @Ni ₂ (OH) ₂ CO ₃ /rGO	HNWAs	785.6 mF cm ⁻² 429.3 F g ⁻¹	10 mA cm ⁻² 5.5 A g ⁻¹	1.01 Wh cm ⁻² 152.6 Wh kg ⁻¹	57.6 W cm ⁻² 3.15 kW kg ⁻¹	Our work

^{a)}PENS: Positive electrode nanostructure

^{b)}AC: Activated carbon

^{c)}HNWAs: Hierarchical nanowire arrays

^{d)}N-C: N-doped carbon

^{e)}HNSAs: Hierarchical nanosheet arrays

^{f)}HMSs: Hollow microspheres

^{g)}CMK: Carbon material from Korea

5

Reference:

- [1] S. Peng, L. Li, H. B. Wu, S. Madhavi, X. W. D. Lou, *Adv. Energy Mater.* **2015**, 5, 1401172-1401179.
- [2] S. Saha, S. Chhetri, P. Khanra, P. Samanta, H. Koo, N. C. Murmu, T. Kuila, *J. Energy Storage* **2016**, 6, 22-31.
- [3] Q. Ke, C. Guan, X. Zhang, M. Zheng, Y. W. Zhang, Y. Cai, H. Zhang, J. Wang, *Adv. Mater.* **2017**, 5, 1604164-1604170.
- [4] Y. Yang, D. Cheng, S. Chen, Y. Guan, J. Xiong, *Electrochim. Acta* **2016**, 193, 116-127.
- [5] C.-H. Tang, X. Yin, H. Gong, *ACS Appl. Mater. Interfaces* **2013**, 5, 10574-10582.
- [6] X. Li, L. Wang, J. Shi, N. Du, G. He, *ACS Appl. Mater. Interfaces* **2016**, 8, 17276-17283.
- [7] K. Xu, R. Zou, W. Li, Q. Liu, X. Liu, L. An, J. Hu, *J. Mater. Chem. A* **2014**, 2, 10090-10097.
- [8] J. Zhu, J. Jiang, Z. Sun, J. Luo, Z. Fan, X. Huang, H. Zhang, T. Yu, *Small* **2014**, 10, 2937-2945.
- [9] K. Xu, W. Li, Q. Liu, B. Li, X. Liu, L. An, Z. Chen, R. Zou, J. Hu, *J. Mater. Chem. A* **2014**, 2, 4795-4802.
- [10] L. Niu, Y. Wang, F. Ruan, C. Shen, S. Shan, M. Xu, Z. Sun, C. Li, X. Liu, Y. Gong, *J. Mater. Chem. A* **2016**, 4, 5669-5677.